

Rethinking Query, Key, and Value Embedding in Vision Transformer under Tiny Model Constraints

Jaesin Ahn[†], Jiuk Hong[†], Jeongwoo Ju[‡] and Heechul Jung[†]

[†]Department of Artificial Intelligence, Kyungpook National University

[‡]Korea Advanced Institute of Science and Technology

{ajs0420, hong4497, heechul}@knu.ac.kr, veryju@kaist.ac.kr

Abstract

A vision transformer (ViT) is the dominant model in the computer vision field. Despite numerous studies that mainly focus on dealing with inductive bias and complexity, there remains the problem of finding better transformer networks. For example, conventional transformer-based models usually use a projection layer for each query (Q), key (K), and value (V) embedding before multi-head self-attention. Insufficient consideration of semantic Q , K , and V embedding may lead to a performance drop. In this paper, we propose three types of structures for Q , K , and V embedding. The first structure utilizes two layers with ReLU, which is a non-linear embedding for Q , K , and V . The second involves sharing one of the non-linear layers to share knowledge among Q , K , and V . The third proposed structure shares all non-linear layers with code parameters. The codes are trainable, and the values determine the embedding process to be performed among Q , K , and V . Hence, we demonstrate the superior image classification performance of the proposed approaches in experiments compared to several state-of-the-art approaches. The proposed method achieved 71.4% with a few parameters (of 3.1M) on the ImageNet-1k dataset compared to that required by the original transformer model of XCiT-N12 (69.9%). Additionally, the method achieved 93.3% with only 2.9M parameters in transfer learning on average for the CIFAR-10, CIFAR-100, Stanford Cars datasets, and STL-10 datasets, which is better than the accuracy of 92.2% obtained via the original XCiT-N12 model.

1. Introduction

Currently, transformers have emerged as dominant models in deep learning because of their superior performance, especially in terms of long-range dependency [7, 30]. Transformers first appeared in natural language processing (NLP) [30] and have since become a widely used backbone

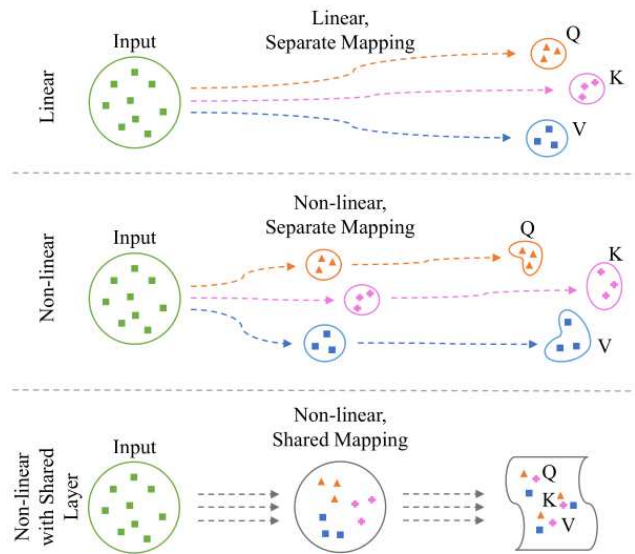


Figure 1. Conceptual diagram of conventional linear mapping, our non-linear mapping, and our non-linear mapping with shared layer. Compared to separate mapping, shared mapping can find a new combination of Q , K , and V in a shared manifold.

network of state-of-the-art models [1, 20, 21]. A transformer mainly adopts a self-attention mechanism with the following feedforward network to capture the sequence of input tokens. The self-attention mechanism can deal with the global information of input tokens, and this feature allows the models to become state-of-the-art models [1, 17].

Although the use of transformers have been increasing in NLP, convolutional neural networks (CNN) have been remained in the mainstream in computer vision (CV) [10, 27, 28, 39]. CNN has representative features such as translation equivariance and spatial locality. These features enable the dominant performance of CNNs in CV tasks [12, 23, 24, 28] such as image classification, object detection, and segmentation; however, recently, transformers have also increased in CV because vision transformers (ViT) [8] offer compet-

itive performance. As current research shows [2, 8, 29], transformer-based networks have now become state-of-the-art models replacing CNN-based networks.

ViT shows superior performance by removing inductive bias, which is a representative feature of CNN and reinforcing long-range dependency. Standard vision transformers flatten 2-dimensional images into 1-dimensional sequences of tokens and then apply a global self-attention mechanism to extract the relation among tokens. This procedure can consider the long-range relationship among tokens, in contrast to CNNs, which consider the local relationship of image pixels. However, it results in extensive computations that increase quadratically according to the image resolution and the need for pre-trained weights [8, 25] using large-scale datasets, that is, JFT-300M [26], ImageNet-21k [6]. To alleviate these inefficiencies, several researchers have considered adding the inductive bias in the transformer explicitly [31, 35, 37, 38], and attempted to reduce the computational cost by modifying the multi-head self-attention (MHSA) method [9]. However, there are few considerations regarding new embedding techniques for query (Q), key (K), and value (V) [31].

In this study, we consider the design of the structure of embedding Q , K , and V . First, we present a two-layer embedding structure model with a rectified linear unit activation function (ReLU). In contrast to the original embedding, the structure can transform the input data into a non-linear space. It has the potential to improve the performance of the ViT because more non-linearity can solve more complicated problems. The second structure is a one-layer shared structure, which is a variant of the first structure. The third structure is a two-layer shared structure with code parameters to improve the original self-attention mechanism used in conventional transformers. Finally, experimental results demonstrate that the proposed method outperforms the state-of-the-art (SOTA) model in the ImageNet [6] classification task and transfer learning on multiple datasets (i.e., CIFAR-10, CIFAR-100 [16], Stanford Cars [15], and STL-10 [4]) for evaluating various image classification tasks.

2. Related Works

ViT was first proposed in Dosovitskiy *et al.* [8]. This pioneering work directly applies a plain transformer encoder, which is commonly used in NLP. They split images into patches to embed them as tokens and feed them to the transformer encoder with additional positional embeddings. The transformer encoder consists of repeated multi-head self-attention and multilayer perceptron (MLP) layers. In contrast to CNN structures, the transformer can handle long-range information by applying global self-attention among the tokens. However, global self-attention causes a lack of inductive bias, which makes large-scale pre-training necessary and quadratically increasing computation. Although

DeiT [29] suggests distilling knowledge using the CNN model as a teacher model to train the transformer without inductive bias, it requires an additional teacher model that causes extra computation.

Therefore, current research mainly focuses on applying explicit inductive bias to vision transformers [5, 18, 33, 37] and reducing the computational complexity from quadratic to linear [9, 13]. XCiT [9] is one study that focused on reducing the computational complexity. It introduces cross-covariance attention (XCA) instead of standard self-attention. XCA effectively reduces computation without a large performance gap compared to the baseline. However, it does not consider Q , K , and V embedding, which directly affects the attention operation. In contrast to these works, we introduce Q , K , and V embedding techniques to improve the performance of image recognition.

CvT [31] is the most similar work conducted before. CvT utilizes convolutional projection for the Q , K , and V embedding of the transformer encoder to take advantage of both the CNN and transformer. However, they also stay to use separate projections and linear operations. This may lead to a constrained combination of Q , K , and V . Although CvT-13 achieved 81.6% in ImageNet classification using 20M parameters and larger models achieved higher scores, they did not consider tiny model constraints.

3. Attention Mechanism in Vision Transformer

ViT [8] constructs the network following the original NLP transformer encoder. It splits images into sets of patches and uses them as tokens, which are embedded with the positional embedding. The embedded vector is used for the following repeated self-attention and feed-forward networks. In this section, we introduce two representative approaches to the self-attention mechanism, namely self-attention and cross-covariance attention.

3.1. Self-attention

Conventional transformers adopt self-attention as the core operation of the network [8, 30]. In the transformer, the input token X is projected by the linear projection layer W_q , W_k , and W_v to embed Q , K , and V vectors, respectively. Then, the dot product V with the attention matrix, which is obtained by the scaled dot product of Q and K . This self-attention operation can be represented as:

$$SA(Q, K, V) = \text{Softmax} \left(\frac{Q \cdot K^T}{\sqrt{d_k}} \right) \cdot V, \quad (1)$$

where $SA(Q, K, V)$ is the output of self-attention and Q , K , V are processed by the following operations:

$$\begin{aligned} Q &= X \cdot W_q, \\ K &= X \cdot W_k, \\ V &= X \cdot W_v, \end{aligned} \quad (2)$$

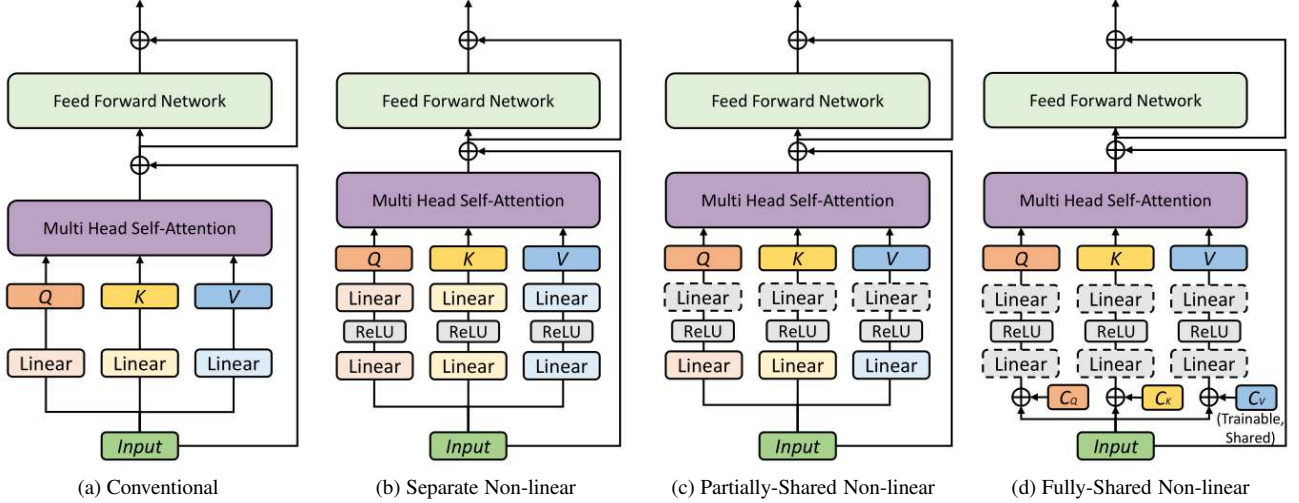


Figure 2. Four types of Q , K , and V embedding methods. (a) The figure depicts conventional embedding used in the standard transformer encoder. (b) Separate non-linear embedding utilizes a two-layer embedding, including non-linearity (ReLU). (c) Partially-shared non-linear embedding includes a weight-sharing linear layer. The weight-sharing layer is depicted as the gray dotted line block, and it follows after the separated linear layer and ReLU. (d) Fully-shared non-linear embedding includes two weight-sharing linear layers, also depicted as a gray dotted line, with ReLU. In this case, trainable codes of Q , K , V (C_q, C_k, C_v) are concatenated to the input tokens.

on $X \in R^{N \times d}$, $W_q \in R^{d \times d_q}$, $W_k \in R^{d \times d_k}$, $W_v \in R^{d \times d_v}$, where N is the number of tokens, and d is the token dimension. Self-attention is usually conducted in a multi-headed manner. When the number of heads is h , $d_q = d_k = d_v = d/h$.

3.2. Cross-covariance Attention

Cross-covariance attention (XCA) is a modified self-attention mechanism that can reduce the computational complexity from $O(N^2d)$ to $O(Nd^2)$. XCiT [9], which is a variant of ViT, suggested the use of XCA instead of standard self-attention operation, which is widely used in transformer networks, demonstrating its SOTA performance in CV tasks, for example, ImageNet classification, self-supervised learning, object detection, and semantic segmentation. They conducted feature dimension self-attention instead of token dimension self-attention, which is used in standard transformer networks. By simply transposing Q, K, V and reversing the order of the dot product, the computational complexity is reduced from quadratic to linear with the number of tokens, N . This transposed feature dimension self-attention can be represented as below:

$$XCA(Q, K, V) = V \cdot \text{Softmax} \left(\frac{\hat{K}^T \cdot \hat{Q}}{\tau} \right), \quad (3)$$

where \hat{Q}, \hat{K} are the l_2 -normalized Q, K vector, and τ is the temperature scaling parameter. This is orthogonal to our research, which proposes to modify the Q, K, V embedding procedure. We adopted XCiT as a baseline model to verify the performance of the proposed method.

4. Proposed method

As mentioned in Eq. 2, the conventional embedding method uses a linear layer for each Q, K , and V . The layer is not shared across the embedding spaces of Q, K , and V . In this paper, we propose three types of new embedding techniques to improve the performance of ViT, as shown in Fig. 2.

4.1. Separate Non-linear Embedding (SNE)

In contrast to the original ViT-based models, we apply non-linear transformations to extract Q, K , and V , respectively, as follows:

$$\begin{aligned} Q &= \sigma(X \cdot W_q^{(1)}) \cdot W_q^{(2)}, \\ K &= \sigma(X \cdot W_k^{(1)}) \cdot W_k^{(2)}, \\ V &= \sigma(X \cdot W_v^{(1)}) \cdot W_v^{(2)}, \end{aligned} \quad (4)$$

where $W_q^{(1)} \in R^{d \times d_q}$ and $W_q^{(2)} \in R^{d_q \times d}$ represent the weight parameters of the first and second fully connected layers, respectively, and the layers encode the input token as Q . $W_k^{(1)} \in R^{d \times d_k}$ and $W_k^{(2)} \in R^{d_k \times d}$ correspond to K , and $W_v^{(1)} \in R^{d \times d_v}$ and $W_v^{(2)} \in R^{d_v \times d}$ extract V . σ is an activation function. Based on the obtained Q, K , and V , Eq. 3 is computed for self-attention.

The layers for the SNE consist of two fully connected layers with an activation function (ReLU) to conduct a non-linear transformation of the input tokens. The non-linear embedding approach may have some advantages. This could increase the total number of non-linearities of the

model. Under the limited number of parameters, the increased number of non-linearities could have a positive effect on improving the generalization. Furthermore, it can expand the search space to find new combinations of Q , K , and V .

4.2. Partially-Shared Non-linear Embedding (P-SNE)

P-SNE shares a layer from two fully connected layers in the SNE model. There are two options for which the layer will be selected (i.e., first or second layers). Sharing the first layer is similar to the linear embedding originally used in the ViT model. The shared first layer produces the same output because the input values are also shared. Consequently, we chose the second layer to be shared among Q , K , and V .

The shared layer linearly transforms each activation value extracted from the first non-linear layer. With the shared layer, Q , K , and V can share knowledge on how to build each token. In addition, separate layers of original or SNE structures might have a potential issue, but the shared layer could prevent this issue. In the separate layers, even if one of the layers responsible for Q , K , and V extraction does not learn well, there might be no problem in minimizing the training loss. This means that the network will be trained well even if one of the three separate layers for Q , K , and V is not updated.

Finally, Q , K , and V in the P-SNE, are extracted as follows:

$$\begin{aligned} Q &= \sigma(X \cdot W_q^{(1)}) \cdot W_s^{(2)}, \\ K &= \sigma(X \cdot W_k^{(1)}) \cdot W_s^{(2)}, \\ V &= \sigma(X \cdot W_v^{(1)}) \cdot W_s^{(2)}, \end{aligned} \quad (5)$$

where $W_s^{(2)} \in R^{d_s \times d}$ denotes the weight parameters of the shared second layer when $d_s = d_q = d_k = d_v$. We replace the weight parameters $W_q^{(2)}$, $W_k^{(2)}$, $W_v^{(2)}$ of the second layer of the SNE with $W_s^{(2)}$.

4.3. Fully-Shared Non-linear Embedding (F-SNE)

For F-SNE, we first integrate Q , K , V projection layers $W_q^{(i)}$, $W_k^{(i)}$, $W_v^{(i)}$ into the shared projection layers $W_s^{(i)}$ for $i = \{1, 2\}$. Instead of Q , K , V projection layers that separately transform input embedding token X into Q , K , V vectors, the shared projection layers transform the input embedding token X into Q , K , V using the shared weight. It can guide the projection of Q , K , and V towards the same manifold.

However, we could only conduct a single transformation using the shared projection layers, which makes it impossible to embed different vectors simultaneously. To handle this problem, we add codes C_q , C_k , C_v to reflect separate

Q , K , and V embedding. C_q , C_k , C_v are trainable vectors that are concatenated to the input token X before passing the shared projection layers W_s . Additionally, the same C_q , C_k , C_v are shared among all the encoders in the transformer. By this sharing, codes will converge at the optimal semantic representation of Q , K , and V that exists consistently regardless of the encoder.

Q , K , V embedding by the proposed shared projection layers with codes C_q , C_k , C_v can be comprehensively represented as follows:

$$\begin{aligned} Q &= \sigma((X \oplus C_q) \cdot W_s^{(1)}) \cdot W_s^{(2)}, \\ K &= \sigma((X \oplus C_k) \cdot W_s^{(1)}) \cdot W_s^{(2)}, \\ V &= \sigma((X \oplus C_v) \cdot W_s^{(1)}) \cdot W_s^{(2)}, \end{aligned} \quad (6)$$

on $X \in R^{N \times d}$ and $C_q, C_k, C_v \in R^{N \times c}$, where \oplus denotes vector concatenation and c is an arbitrary code size. Here, $C_q, C_k, C_v \in R^{1 \times c}$, but they are repeated N times to match the dimension. The codes C_q , C_k , and C_v are computed to minimize the loss function as follows:

$$\hat{C}_q, \hat{C}_k, \hat{C}_v = \min_{C_q, C_k, C_v} \mathcal{L}(D; \theta, C_q, C_k, C_v) + \lambda \mathcal{R}(\theta), \quad (7)$$

where \mathcal{L} is a loss function used in the transformer (i.e., cross-entropy loss). θ denotes the total parameters of the transformer network, and D is the training set. \mathcal{R} represents a regularizer (i.e., weight decay), and λ is a parameter that controls the strength of the regularizer.

5. Experiments and Results

We evaluated the effect of the new Q , K , and V embedding methods on image classification tasks. We first evaluated the performance of the proposed structures with the ImageNet-1k dataset and then used those models to transfer to the other datasets (i.e., CIFAR-10, CIFAR-100, Stanford Cars, and STL-10). Additionally, we conducted brief experiments using distillation when we evaluated the performance of the models with the ImageNet-1k dataset.

All the experiments for our methods were conducted using XCiT-Nano and XCiT-Tiny models, which were introduced in [9] as the baseline models. In the following sections, we use the brief notations XCiT-N12 and XCiT-T12 to describe the XCiT-Nano and XCiT-Tiny models with 12 repeated encoders. While the input image size of the models was fixed at 224×224 , we trained the models using a batch size of 4,096 for XCiT-N12-based models and 2,816 for XCiT-T12-based models. For ImageNet training, we trained the model for 400 epochs with an initial learning rate of 5×10^{-4} . For transfer learning, we used an initial learning rate of 5×10^{-5} for 1,000 epochs of training. We followed other experimental setups of the original XCiT. Overall experiments were conducted on NVIDIA DGX A100 (8 GPUs).

For the Q , K , and V projection layers, we used the output dimensions depicted in Table 1 according to the variants. Additionally, in the case of the XCI-T-N12 (F-SNE, c) model, the shared projection layers have an input dimension of $(128 + c)$ to take the input concatenated with the code, and the XCI-T-T12 (F-SNE, c) model has shared projection layers with an input dimension of $(192 + c)$. Code is a parameter vector of arbitrary code size (e.g., $c = 8, 16, 32, 64$) defined outside the encoder to be shared among the encoders. For a fair comparison, we compare the number of parameters as well as the performance in the following sections. In the case of the F-SNE models, codes were also included in the model parameters.

Table 1. Corresponding output dimensions of Q, K, V embedding layers to each model variant.

Model	Nano		Tiny	
	d	d_q, d_k, d_v	d	d_q, d_k, d_v
XCI-T [9]	128	128	192	192
XCI-T (SNE)	128	64	192	96
XCI-T (P-SNE)	128	96	192	144
XCI-T (F-SNE, c)	128	128	192	192
XCI-T (F-SNE, 8*)	128	186	192	282
XCI-T (F-SNE, 16*)	128	182	192	276

5.1. ImageNet Classification

Table 2 shows the ImageNet classification results to compare other models with our proposed method. Top-1 accuracies from other models noted in the table came directly from each model’s publications. In this section, we used ImageNet-1k, which consists of 1.28M training images and 50,000 validation images with 1,000 labels. To demonstrate the performance of the proposed method, we selected XCI-T as a baseline model and modified Q , K , and V projection layers corresponding to each model variant.

As shown in Table 2, the P-SNE model achieved the best score for the below 4M parameters constraints, improving the accuracy by 1.5% from the baseline. Even in the case of the below 10M parameters constraints, the P-SNE model surpassed the previous SOTA model, which recorded 77.3% top-1 accuracy while improving the accuracy by 0.5% from it. The starred (*) model is an additional experiment to compare the performance of our method using the same number of parameters as the original XCI-T model. This shows that the performance can be improved by adding parameters to the embedding layers as much as the capacity saved by fully sharing the embedding layers. For example, the XCI-T-T12 (F-SNE, 8*) model scored 77.7%, which is close to the best accuracy of 77.8%. Moreover, the non-linear embedding method (SNE) also improves the classification rates on the ImageNet dataset, compared to the baseline model which uses the linear embedding method.

Table 2. Evaluation on ImageNet classification task with <10M parameters. In Type, ‘C’ denotes CNN architecture, and ‘T’ denotes the transformer architecture. Gray color represents our methods.

Model	param #	Type	Top-1 (%)
Mobile-Former-26M [3]	3.2M	C+T	64.0
Mobile-Former-52M [3]	3.5M	C+T	68.7
MobileNetV3-S [12]	2.5M	C	67.4
MobileNetV3-S/1.25x [12]	3.6M	C	70.4
XCI-T-N12 (baseline) [9]	3.1M	T	69.9
XCI-T-N12 (SNE)	3.1M	T	70.9 (+1.0)
XCI-T-N12 (P-SNE)	3.1M	T	71.4 (+1.5)
XCI-T-N12 (F-SNE, 8)	2.9M	T	70.6 (+0.7)
XCI-T-N12 (F-SNE, 8*)	3.1M	T	70.8 (+0.9)
XCI-T-N12 (F-SNE, 16)	2.9M	T	70.2 (+0.3)
XCI-T-N12 (F-SNE, 16*)	3.1M	T	70.6 (+0.7)
XCI-T-N12 (F-SNE, 32)	2.9M	T	70.3 (+0.4)
XCI-T-N12 (F-SNE, 64)	2.9M	T	70.2 (+0.3)
ViT-Ti [8]	5.7M	T	68.7
T2T-ViT-7 [37]	4.3M	T	71.7
DeiT-Ti [29]	5.7M	T	72.2
Mobile-Former-96M [3]	4.6M	C+T	72.8
LocalViT-T2T [18]	4.3M	C+T	72.5
PiT-Ti [11]	4.9M	C+T	73.0
ConViT-Ti [5]	5.7M	C+T	73.1
ConT-Ti [34]	5.8M	C+T	74.9
LocalViT-T [18]	5.9M	C+T	74.8
ViTAE-T [33]	4.8M	C+T	75.3
EfficientNet-B0 [28]	5.3M	C	76.3
CeiT-T [36]	6.4M	C+T	76.4
T2T-ViT-12 [37]	6.9M	T	76.5
ConT-S [34]	10.1M	C+T	76.5
CoaT-Lite Tiny [32]	5.7M	C+T	76.6
Swin-1G [3, 19]	7.3M	T	77.3
XCI-T-T12 (baseline) [9]	6.7M	T	77.1
XCI-T-T12 (SNE)	6.7M	T	77.6 (+0.5)
XCI-T-T12 (P-SNE)	6.7M	T	77.8 (+0.7)
XCI-T-T12 (F-SNE, 8)	6.3M	T	76.8 (-0.3)
XCI-T-T12 (F-SNE, 8*)	6.7M	T	77.7 (+0.6)
XCI-T-T12 (F-SNE, 16)	6.3M	T	77.2 (+0.1)
XCI-T-T12 (F-SNE, 16*)	6.7M	T	77.4 (+0.3)
XCI-T-T12 (F-SNE, 32)	6.3M	T	77.1 (0.0)
XCI-T-T12 (F-SNE, 64)	6.3M	T	77.1 (0.0)

5.2. Distillation

We evaluated the performances on ImageNet classification task using distillation technique as well. In this section, we used RegNetY-16GF [22] as a teacher model to conduct hard distillation as proposed in [29]. Similar to the previous experimental results in [9, 29], distillation could improve the performance of each model. Additionally, shared non-linear embedding methods improve the performance of the baseline model, although a separate non-linear embedding method decreases the performance. This reminds us of the better properties of the shared embedding methods, which

is consistent with the results shown in the previous section. These results are organized in Table 3.

Table 3. Evaluation on ImageNet classification with distillation. Gray color represents our methods.

Model	param #	Top-1 (%)
XCiT-N12 (baseline)§ [9]	3.1M	71.7
XCiT-N12 (SNE)§	3.1M	71.5 (-0.2)
XCiT-N12 (P-SNE)§	3.1M	71.9 (+0.2)
XCiT-N12 (F-SNE, 8)§	2.9M	71.7 (0.0)
XCiT-N12 (F-SNE, 8*)§	3.1M	72.4 (+0.7)
XCiT-N12 (F-SNE, 16)§	2.9M	72.0 (+0.3)
XCiT-N12 (F-SNE, 16*)§	3.1M	72.2 (+0.5)
XCiT-N12 (F-SNE, 32)§	2.9M	71.9 (+0.2)
XCiT-N12 (F-SNE, 64)§	2.9M	71.8 (+0.1)

5.3. Transfer Learning

To demonstrate the generalization performance of our method, we conducted transfer learning experiments on CIFAR-10, CIFAR-100 [16], Stanford Cars [15], and STL-10 [4] datasets as shown in Table 4. CIFAR-10 and CIFAR-100 consist of 50,000 training images and 10,000 test images with 10 and 100 classes, respectively. The Stanford Cars dataset consists of 8,144 training images and 8,041 test images of 196 classes. Lastly, we used the STL-10 dataset, which contains 5,000 training images and 8,000 test images from 10 classes.

As shown in the average score of Table 4, our method generally improves the performance of the baseline model. In particular, XCiT-N12 (F-SNE, 32) and XCiT-T12 (F-SNE, 8) achieved the best score under each parameter constraint, below 4M and 10M, despite having fewer parameters. Including these best models, F-SNE models showed mostly better transfer performance compared to other variants on average. It can be assumed that fully shared embedding may provide better generalization capability than other variants. However, on the Cars dataset, there were performance drops in the case of transferring XCiT-T12-based models, as opposed to the case of transferring XCiT-N12-based models. The embedding dimension of XCiT-T12 is larger than that of XCiT-N12, which means that XCiT-T12 has an extra capacity to find a complex mapping function. It may decrease the contribution of non-linear embeddings. However, it is still worth using non-linear embedding methods in small models.

6. Ablation Study and Analysis

We performed several ablation studies to analyze the proposed embedding structures, such as variation in the number of non-linear layers, comparison of shared and unshared code, code visualization of F-SNE, and code size search.

6.1. Impact of the Number of Layers

All the proposed methods utilize the two-layer model for non-linear embedding, which is the smallest unit that expresses non-linearity. To analyze the impact of the number of layers, we performed an analysis according to the number of layers. Fig. 3 shows the results based on the XCiT-N12 (SNE) model using the ImageNet dataset.

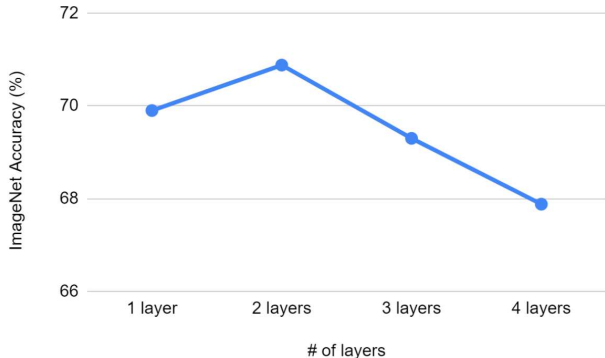


Figure 3. Performance comparison between the number of non-linear layers from 1 to 4. The two layers achieved the best accuracy, while three or four layers showed lower accuracies.

The accuracies with three or four layers decreased, but the best accuracy was achieved when two layers were used. Based on the results, we conclude that more than a single non-linearity embedding can hinder the embedding performance in terms of accuracy.

6.2. Sharing or Unsharing Codes in F-SNE

Owing to the code, the input token can be identified in the F-SNE for separately extracting Q , K , and V . In the F-SNE model, codes C_q , C_k , and C_v are shared across all embedding modules in the transformer model. This is effective for slightly decreasing the total number of parameters. In addition, as shown in Table 5, the performance can be improved. Without sharing, the codes might have different values, which could hinder to find the optimal code vectors for Q , K , and V . Sharing might be a good prior knowledge to reach the optimal solution.

Table 5. Comparison between the cases of code sharing and un-sharing tested on the ImageNet dataset. The numbers in brackets denote the total number of parameters for each model.

Model	Sharing	W/o sharing
XCiT-N12 (F-SNE, 8*)	70.82 (2.9M)	70.28 (3.05M)

6.3. C_q , C_k , and C_v in Different Tasks

The optimal code values were initially found on the ImageNet dataset, and then the computed code values were used as the initial codes for the downstream tasks. Even

Table 4. Evaluation on transfer learning. All models were pre-trained using the ImageNet-1k dataset. † indicates the results are obtained from the paper. ‡ indicates that the experiment cannot be performed due to the lack of source code. Gray color represents our methods.

Model	param #	CIFAR-10 (%)	CIFAR-100 (%)	Cars (%)	STL-10 (%)	Average (%)
MobileNetV3-S [12]	2.9M	96.6	82.3	79.8	94.3	88.3
MobileNetV3-L/0.75x [12]	4.0M	97.5	84.9	87.6	96.5	91.6
RegNetY-200MF [22]	3.2M	97.4	84.2	86.3	96.2	91.0
RegNetY-400MF [22]	4.3M	97.8	84.6	90.7	97.0	92.5
EfficientNet-B0 [28]	5.3M	98.1 [†]	88.1 [†]	90.8	98.1	93.8
ViTAE-T [33]	4.8M	97.3 [†]	86.0 [†]	89.5 [†]	- [‡]	-
CeiT-T [36]	6.4M	98.5 [†]	88.4[†]	90.5 [†]	98.3	93.9
XCiT-N12 (baseline) [9]	3.1M	98.0	85.5	87.9	97.5	92.2
XCiT-N12 (SNE)	3.1M	98.4 (+0.4)	86.6 (+1.1)	88.9 (+1.0)	97.8 (+0.3)	92.9 (+0.7)
XCiT-N12 (P-SNE)	3.1M	98.2 (+0.2)	86.5 (+1.0)	88.9 (+1.0)	97.9 (+0.4)	92.9 (+0.7)
XCiT-N12 (F-SNE, 8)	2.9M	98.1 (+0.1)	86.2 (+0.7)	89.0 (+1.1)	97.8 (+0.3)	92.8 (+0.6)
XCiT-N12 (F-SNE, 8*)	3.1M	98.3 (+0.3)	86.2 (+0.7)	89.0 (+1.1)	97.8 (+0.3)	92.8 (+0.6)
XCiT-N12 (F-SNE, 16)	2.9M	98.2 (+0.2)	86.3 (+0.8)	90.2 (+2.3)	97.8 (+0.3)	93.1 (+0.9)
XCiT-N12 (F-SNE, 16*)	3.1M	98.3 (+0.3)	86.3 (+0.8)	90.5 (+2.6)	97.9 (+0.4)	93.2 (+1.0)
XCiT-N12 (F-SNE, 32)	2.9M	98.1 (+0.1)	86.8 (+1.3)	90.6 (+2.7)	97.8 (+0.3)	93.3 (+1.1)
XCiT-N12 (F-SNE, 64)	2.9M	98.1 (+0.1)	86.2 (+0.7)	89.1 (+1.2)	97.6 (+0.1)	92.8 (+0.6)
XCiT-T12 (baseline) [9]	6.7M	98.5	86.7	92.7	98.3	94.0
XCiT-T12 (SNE)	6.7M	98.6 (+0.1)	87.2 (+0.5)	91.8 (-0.9)	98.6 (+0.3)	94.0 (0.0)
XCiT-T12 (P-SNE)	6.7M	98.7 (+0.2)	87.2 (+0.5)	91.8 (-0.9)	98.6 (+0.3)	94.1 (+0.1)
XCiT-T12 (F-SNE, 8)	6.3M	98.4 (-0.1)	88.0 (+1.3)	92.3 (-0.4)	98.6 (+0.3)	94.3 (+0.3)
XCiT-T12 (F-SNE, 8*)	6.7M	98.5 (0.0)	87.6 (+0.9)	92.1 (-0.6)	98.3 (0.0)	94.1 (+0.1)
XCiT-T12 (F-SNE, 16)	6.3M	98.5 (0.0)	87.2 (+0.5)	92.3 (-0.4)	98.7 (+0.4)	94.2 (+0.2)
XCiT-T12 (F-SNE, 16*)	6.3M	98.6 (+0.1)	87.8 (+1.1)	92.3 (-0.4)	98.6 (+0.3)	94.3 (+0.3)
XCiT-T12 (F-SNE, 32)	6.3M	98.5 (0.0)	87.9 (+1.2)	92.3 (-0.4)	98.4 (+0.1)	94.3 (+0.3)
XCiT-T12 (F-SNE, 64)	6.4M	98.5 (0.0)	87.7 (+1.0)	92.3 (-0.4)	98.5 (+0.2)	94.3 (+0.3)

if the pre-trained codes are used, the code values might vary according to the tasks because the codes are updated via a back-propagation process using the downstream task dataset.

Figure 4 shows correlation values of the codes extracted from each downstream task. Interestingly, the correlation matrices are very similar even if the task is changed. The diagonal elements give some information on the similarity between the same codes, and non-diagonal elements depict the similarity between different codes. Non-diagonal elements are close to the zero, and each code of C_q , C_k , and C_v tends to have the property of orthogonality. These results can be interpreted that C_q , C_k , and C_v learn their inherent feature to be used as Q , K , and V , regardless of the task; furthermore, the values of the l_2 -norm for each dataset can be obtained, as presented in Table 6. The codes of ImageNet, Cars, and STL-10 have similar l_2 -norm values, but CIFAR-10 and 100 have different l_2 -norm values.

6.4. Do Better ImageNet Models Transfer Better?

In general, better ImageNet models transfer better [14]. An experiment was conducted to verify whether this fact also applies to our cases. As shown in Fig. 5, we could observe correlation between performances on ImageNet and on downstream tasks. The correlation tendency is reflected

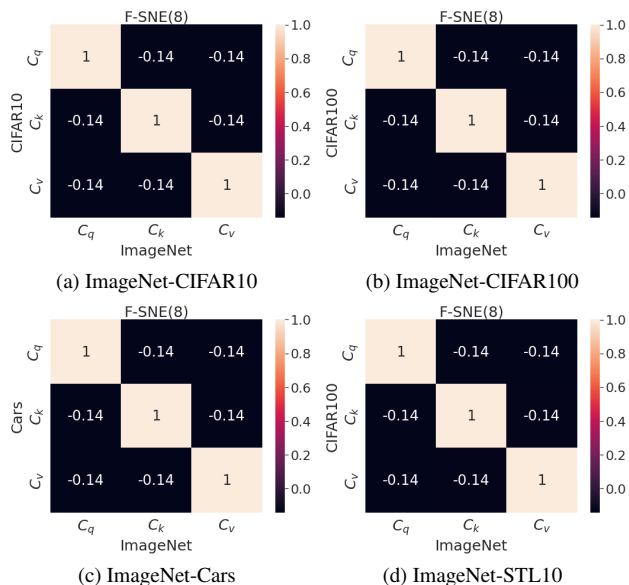


Figure 4. Dot product value of l_2 -normalized C_q , C_k , and C_v according to the trained datasets. C_q , C_k , and C_v are extracted from the XCiT-N12 (F-SNE, 8) model.

by the domain difference between the upstream and downstream tasks. In other words, the tasks of the CIFAR and

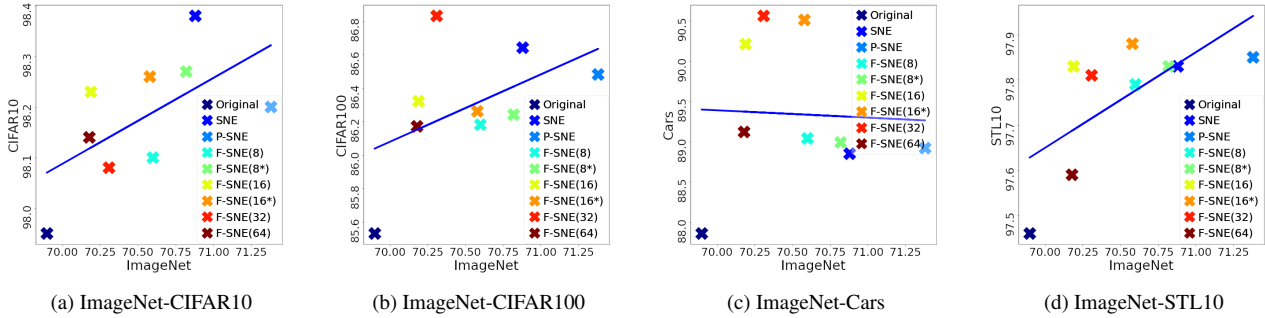


Figure 5. Correlation plots of pre-training and transfer learning performances. XCiT-N12-based models are used. 'X' markers denote the accuracies of each model, and the blue line denotes the regression slope of the results. In contrast to other correlated plots, the results on the Cars dataset are not correlated with the results on the ImageNet dataset. Best viewed in color.

Table 6. l_2 -norm of C_q , C_k , and C_v extracted from XCiT-N12 (F-SNE, 8) model according to the trained dataset.

Dataset	$\ C_q\ $	$\ C_k\ $	$\ C_v\ $
ImageNet	8.86	8.13	8.53
CIFAR-10	9.05	8.34	8.74
CIFAR-100	9.06	8.35	8.77
Cars	8.84	8.13	8.53
STL-10	8.86	8.14	8.56

STL datasets are similar to the task of ImageNet, so they show high correlations between two tasks. However, in the Stanford Cars dataset, it is difficult to see the correlations.

6.5. Code Size

It is important to select an appropriate code size to utilize the code C_q , C_k , and C_v in the F-SNE model. We conducted the experiments for the code size, from 8 to 64, to find an appropriate code size that leads to better performance. As shown in Figure 6, the code size of 8 achieved the best accuracy between the nano models and 16 achieved the best accuracy between the tiny models. The tiny models have an embedding dimension of about 1.5 times the embedding dimension of the nano models, as shown in Table 1. It can be interpreted that it requires a larger code size when the embedding dimension of the model gets larger.

7. Limitations

The limitations of our work are considered in two aspects: performance and constraint. In terms of performance, our approaches are degraded in the Stanford Cars dataset with the XCiT-T12 model, as shown in Table 4. For the constraint, we started with the constraints of the small models. However, our approach can also be applied to other large models, and we believe that small modifications can make our structures easily applicable to large models.

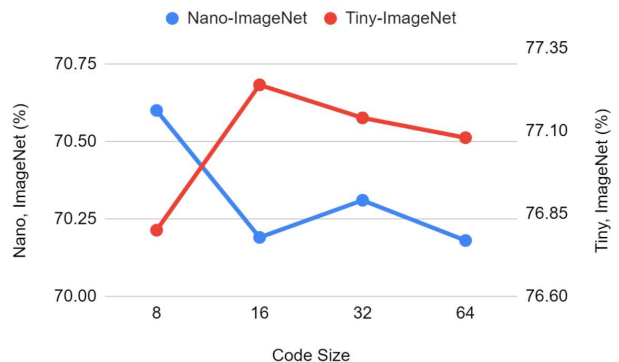


Figure 6. ImageNet classification top-1 accuracy of nano (Nano-ImageNet) and tiny (Tiny-ImageNet) models with respect to the code size from 8 to 64. The nano models correspond to the left axis, and the tiny models correspond to the right axis. Best viewed in color.

8. Conclusion

In this paper, we proposed three new types of Q , K , and V vector embedding structures for ViT. The first embedding structure utilizes two non-linear layers to embed the input token into separate non-linear spaces of Q , K , and V . The second structure shares a single layer between the two layers. Based on experiments, we observed that sharing a single layer is effective for ImageNet classification. The third structure shares two layers with the Q , K , and V codes. The codes are trained via a back-propagation algorithm to minimize the loss of ViT. The structure is helpful for improving the classification rates in several downstream tasks, such as CIFAR-100 and STL-10. We could easily improve the XCiT model, which is a representative ViT model, using the proposed structures. In particular, our structures performed well with a small number of parameters (approximately 3M or 6M), but we could not prove the effectiveness of the structures in large models. Some modifications may be required to apply the proposed structures to large models; however, we believe that our research is valuable because it can be the starting point for future studies in this direction.

References

- [1] Tom B Brown, Benjamin Mann, Nick Ryder, Melanie Subbiah, Jared Kaplan, Prafulla Dhariwal, Arvind Neelakantan, Pranav Shyam, Girish Sastry, Amanda Askell, et al. Language models are few-shot learners. *arXiv preprint arXiv:2005.14165*, 2020. 1
- [2] Nicolas Carion, Francisco Massa, Gabriel Synnaeve, Nicolas Usunier, Alexander Kirillov, and Sergey Zagoruyko. End-to-End object detection with transformers. In *Computer Vision – ECCV 2020*, pages 213–229. Springer International Publishing, 2020. 2
- [3] Yinpeng Chen, Xiyang Dai, Dongdong Chen, Mengchen Liu, Xiaoyi Dong, Lu Yuan, and Zicheng Liu. Mobileformer: Bridging mobilenet and transformer. *arXiv preprint arXiv:2108.05895*, 2021. 5
- [4] Adam Coates, Andrew Ng, and Honglak Lee. An analysis of single-layer networks in unsupervised feature learning. In *Proceedings of the fourteenth international conference on artificial intelligence and statistics*, pages 215–223. JMLR Workshop and Conference Proceedings, 2011. 2, 6
- [5] Stéphane d’Ascoli, Hugo Touvron, Matthew Leavitt, Ari Morcos, Giulio Biroli, and Levent Sagun. Convit: Improving vision transformers with soft convolutional inductive biases. *arXiv preprint arXiv:2103.10697*, 2021. 2, 5
- [6] Jia Deng, Wei Dong, Richard Socher, Li-Jia Li, Kai Li, and Li Fei-Fei. ImageNet: A large-scale hierarchical image database. In *2009 IEEE Conference on Computer Vision and Pattern Recognition*, pages 248–255. ieeexplore.ieee.org, June 2009. 2
- [7] Jacob Devlin, Ming-Wei Chang, Kenton Lee, and Kristina Toutanova. BERT: Pre-training of deep bidirectional transformers for language understanding. In *Proceedings of the 2019 Conference of the North American Chapter of the Association for Computational Linguistics: Human Language Technologies, Volume 1 (Long and Short Papers)*, pages 4171–4186. Association for Computational Linguistics, Oct. 2018. 1
- [8] Alexey Dosovitskiy, Lucas Beyer, Alexander Kolesnikov, Dirk Weissenborn, Xiaohua Zhai, Thomas Unterthiner, Mostafa Dehghani, Matthias Minderer, Georg Heigold, Sylvain Gelly, et al. An image is worth 16x16 words: Transformers for image recognition at scale. *arXiv preprint arXiv:2010.11929*, 2020. 1, 2, 5
- [9] Alaaeldin El-Nouby, Hugo Touvron, Mathilde Caron, Piotr Bojanowski, Matthijs Douze, Armand Joulin, Ivan Laptev, Natalia Neverova, Gabriel Synnaeve, Jakob Verbeek, and Hervé Jegou. XcIT: Cross-Covariance image transformers. <http://arxiv.org/abs/2106.09681>, June 2021. 2, 3, 4, 5, 6, 7
- [10] Kaiming He, Xiangyu Zhang, Shaoqing Ren, and Jian Sun. Deep residual learning for image recognition. In *Proceedings of the IEEE conference on computer vision and pattern recognition*, pages 770–778. openaccess.thecvf.com, 2016. 1
- [11] Byeongho Heo, Sangdoon Yun, Dongyoon Han, Sanghyuk Chun, Junsuk Choe, and Seong Joon Oh. Rethinking spatial dimensions of vision transformers. *arXiv preprint arXiv:2103.16302*, 2021. 5
- [12] Andrew Howard, Mark Sandler, Grace Chu, Liang-Chieh Chen, Bo Chen, Mingxing Tan, Weijun Wang, Yukun Zhu, Ruoming Pang, Vijay Vasudevan, and Others. Searching for mobilenetv3. In *Proceedings of the IEEE/CVF International Conference on Computer Vision*, pages 1314–1324. openaccess.thecvf.com, 2019. 1, 5, 7
- [13] Andrew Jaegle, Felix Gimeno, Andrew Brock, Andrew Zisserman, Oriol Vinyals, and Joao Carreira. Perceiver: General perception with iterative attention. *arXiv preprint arXiv:2103.03206*, 2021. 2
- [14] Simon Kornblith, Jonathon Shlens, and Quoc V Le. Do better imagenet models transfer better? In *Proceedings of the IEEE/CVF Conference on Computer Vision and Pattern Recognition*, pages 2661–2671, 2019. 7
- [15] Jonathan Krause, Michael Stark, Jia Deng, and Li Fei-Fei. 3d object representations for fine-grained categorization. In *Proceedings of the IEEE international conference on computer vision workshops*, pages 554–561. cv-foundation.org, 2013. 2, 6
- [16] Alex Krizhevsky, Geoffrey Hinton, et al. Learning multiple layers of features from tiny images. Technical report, 2009. 2, 6
- [17] Mike Lewis, Yinhan Liu, Naman Goyal, Marjan Ghazvininejad, Abdelrahman Mohamed, Omer Levy, Ves Stoyanov, and Luke Zettlemoyer. BART: Denoising Sequence-to-Sequence pre-training for natural language generation, translation, and comprehension. In *Proceedings of the 58th Annual Meeting of the Association for Computational Linguistics*, pages 7871–7880. Association for Computational Linguistics, Oct. 2019. 1
- [18] Yawei Li, Kai Zhang, Jiezhong Cao, Radu Timofte, and Luc Van Gool. Localvit: Bringing locality to vision transformers. *arXiv preprint arXiv:2104.05707*, 2021. 2, 5
- [19] Ze Liu, Yutong Lin, Yue Cao, Han Hu, Yixuan Wei, Zheng Zhang, Stephen Lin, and Baining Guo. Swin transformer: Hierarchical vision transformer using shifted windows. *arXiv preprint arXiv:2103.14030*, 2021. 5
- [20] Alec Radford, Karthik Narasimhan, Tim Salimans, and Ilya Sutskever. Improving language understanding by generative pre-training. <https://www.cs.ubc.ca/~amuham01/LING530/papers/radford2018>. Accessed: 2021-10-13. 1
- [21] Alec Radford, Jeffrey Wu, Rewon Child, David Luan, Dario Amodei, Ilya Sutskever, and Others. Language models are unsupervised multitask learners. *OpenAI blog*, 1(8):9, 2019. 1
- [22] Ilija Radosavovic, Raj Prateek Kosaraju, Ross Girshick, Kaiming He, and Piotr Dollár. Designing network design spaces. In *Proceedings of the IEEE/CVF Conference on Computer Vision and Pattern Recognition*, pages 10428–10436, 2020. 5, 7
- [23] Joseph Redmon, Santosh Divvala, Ross Girshick, and Ali Farhadi. You only look once: Unified, real-time object detection. In *Proceedings of the IEEE conference on computer vision and pattern recognition*, pages 779–788. cv-foundation.org, 2016. 1

- [24] Olaf Ronneberger, Philipp Fischer, and Thomas Brox. U-net: Convolutional networks for biomedical image segmentation. In *International Conference on Medical image computing and computer-assisted intervention*, pages 234–241. Springer, 2015. [1](#)
- [25] Andreas Steiner, Alexander Kolesnikov, Xiaohua Zhai, Ross Wightman, Jakob Uszkoreit, and Lucas Beyer. How to train your vit? data, augmentation, and regularization in vision transformers. *arXiv preprint arXiv:2106.10270*, 2021. [2](#)
- [26] Chen Sun, Abhinav Shrivastava, Saurabh Singh, and Abhinav Gupta. Revisiting unreasonable effectiveness of data in deep learning era. In *Proceedings of the IEEE international conference on computer vision*, pages 843–852, 2017. [2](#)
- [27] Christian Szegedy, Wei Liu, Yangqing Jia, Pierre Sermanet, Scott Reed, Dragomir Anguelov, Dumitru Erhan, Vincent Vanhoucke, and Andrew Rabinovich. Going deeper with convolutions. In *Proceedings of the IEEE Computer Society Conference on Computer Vision and Pattern Recognition*, volume 07-12-June, pages 1–9, Sept. 2015. [1](#)
- [28] Mingxing Tan and Quoc Le. Efficientnet: Rethinking model scaling for convolutional neural networks. In *International Conference on Machine Learning*, pages 6105–6114. proceedings.mlr.press, 2019. [1](#), [5](#), [7](#)
- [29] Hugo Touvron, Matthieu Cord, Matthijs Douze, Francisco Massa, Alexandre Sablayrolles, and Hervé Jégou. Training data-efficient image transformers & distillation through attention, Dec. 2020. [2](#), [5](#)
- [30] Ashish Vaswani, Noam Shazeer, Niki Parmar, Jakob Uszkoreit, Llion Jones, Aidan N Gomez, Łukasz Kaiser, and Illia Polosukhin. Attention is all you need. In *Advances in neural information processing systems*, pages 5998–6008. papers.nips.cc, 2017. [1](#), [2](#)
- [31] Haiping Wu, Bin Xiao, Noel Codella, Mengchen Liu, Xiyang Dai, Lu Yuan, and Lei Zhang. Cvt: Introducing convolutions to vision transformers. *arXiv preprint arXiv:2103.15808*, 2021. [2](#)
- [32] Weijian Xu, Yifan Xu, Tyler Chang, and Zhuowen Tu. Co-scale conv-attentional image transformers. *arXiv preprint arXiv:2104.06399*, 2021. [5](#)
- [33] Yufei Xu, Qiming Zhang, Jing Zhang, and Dacheng Tao. Vi-tae: Vision transformer advanced by exploring intrinsic inductive bias. *arXiv preprint arXiv:2106.03348*, 2021. [2](#), [5](#), [7](#)
- [34] Haotian Yan, Zhe Li, Weijian Li, Changhu Wang, Ming Wu, and Chuang Zhang. Contnet: Why not use convolution and transformer at the same time? *arXiv preprint arXiv:2104.13497*, 2021. [5](#)
- [35] Jianwei Yang, Chunyuan Li, Pengchuan Zhang, Xiyang Dai, Bin Xiao, Lu Yuan, and Jianfeng Gao. Focal self-attention for local-global interactions in vision transformers. *arXiv preprint arXiv:2107.00641*, 2021. [2](#)
- [36] Kun Yuan, Shaopeng Guo, Ziwei Liu, Aojun Zhou, Fengwei Yu, and Wei Wu. Incorporating convolution designs into visual transformers. *arXiv preprint arXiv:2103.11816*, 2021. [5](#), [7](#)
- [37] Li Yuan, Yunpeng Chen, Tao Wang, Weihao Yu, Yujun Shi, Zihang Jiang, Francis EH Tay, Jiashi Feng, and Shuicheng Yan. Tokens-to-token vit: Training vision transformers from scratch on imagenet. *arXiv preprint arXiv:2101.11986*, 2021. [2](#), [5](#)
- [38] Li Yuan, Qibin Hou, Zihang Jiang, Jiashi Feng, and Shuicheng Yan. Volo: Vision outlooker for visual recognition. *arXiv preprint arXiv:2106.13112*, 2021. [2](#)
- [39] Barret Zoph, Vijay Vasudevan, Jonathon Shlens, and Quoc V Le. Learning transferable architectures for scalable image recognition. In *Proceedings of the IEEE conference on computer vision and pattern recognition*, pages 8697–8710. openaccess.thecvf.com, 2018. [1](#)